Article

Molecular Imprinting on Inorganic Nanozymes for Hundred-fold Enzyme Specificity

Zijie Zhang, Xiaohan Zhang, Biwu Liu, and Juewen Liu

J. Am. Chem. Soc., **Just Accepted Manuscript** • DOI: 10.1021/jacs.7b00601 • Publication Date (Web): 27 Mar 2017

Molecular Imprinting on Inorganic Nanozymes for Hundred-fold Enzyme Specificity

Zijie Zhang, Xiaohan Zhang, Biwu Liu, and Juewen Liu*

Department of Chemistry, Waterloo Institute for Nanotechnology, University of Waterloo, Waterloo, Ontario, Canada, N2L 3G1.

Supporting Information Placeholder

ABSTRACT: Enzyme-mimicking nanomaterials (nanozymes) are more cost-effective and robust than protein enzymes, but they lack specificity. Herein, molecularly imprinted polymers were grown on Fe_3O_4 nanozymes with peroxidase-like activity to create substrate binding pockets. Electron microscopy confirmed a shell of nanogel. By imprinting with an adsorbed substrate, moderate specificity was achieved with neutral monomers. Further introducing charged monomers led to nearly 100-fold specificity for the imprinted substrate over the non-imprinted compared to that of bare Fe_3O_4. Selective substrate binding was further confirmed by isothermal titration calorimetry. The same method was also successfully applied for imprinting on gold nanoparticles (peroxidase mimics) and nanoceria (oxidase mimics). Molecular imprinting furthers the functional enzyme mimicking aspect of nanozymes, and such hybrid materials will find applications in biosensor development, separation, environmental remediation, and drug delivery.

Introduction

Nanozymes refer to nanomaterials that catalyze enzyme-like reactions under near physiological conditions.[1-7] With much higher stability and lower cost than protein enzymes, nanozymes are attractive for various applications ranging from biosensor development,[8-11] environmental remediation,[12,13] to nanomedicine.[14-19] In the past few decades, a diverse range of nanomaterials were discovered with oxidase,[9,11,20,21] peroxidase,[1,22-24] catalase,[25] superoxide dismutase,[26] and laccase mimicking activities.[27]

While most previous work focused on catalytic activity, substrate specificity of nanozymes has yet to be addressed. Nanozymes do not have a substrate binding pocket, a feature of most natural enzymes. Since nanozymes' reactions take place on their surfaces, substrates diffused to the surface can all react regardless of their shape and charge. Therefore, most nanozymes can turnover a diverse range of substrates. Substrate specificity is an important feature of enzymes, enabling its molecular recognition function. As such, a critical step towards real enzyme mimics is to engineer substrate binding pockets. Many methods can be potentially used, such as attaching aptamers, peptides, or antibodies.[28] Using these biological ligands, however, defeats the cost and stability advantages of nanozymes.

Molecularly imprinted polymers (MIPs) are created by polymerizing monomers around a template molecule.[29] The chosen monomers often complement to the property of the template to form pre-polymer binding complexes.[30-32] Upon polymerization, the template is imprinted by the crosslinked polymer matrix. After removing the template, a cavity is then produced for rebinding the template. MIPs are also called plastic antibodies to highlight their specific binding and cost-effective polymeric nature.[33,34] We reason that MIPs might be ideal for creating substrate binding cavities on nanozymes since both can be prepared at a large scale and low cost.[35-38]

Molecular imprinting was previously performed on an esterase mimic to increase catalytic activity,[39] and also on a DNA-based enzyme.[40] In those cases, a covalent linkage was made between the enzymes and the MIPs. For nanozymes, covalent grafting MIPs is more difficult and entrapment is preferred. We herein grew MIPs on three classic nanozymes with peroxidase and oxidase like activities. This simple method has achieved remarkable specificity as well as activity enhancement.

Materials and Methods

Chemicals. 3,3',5,5'-tetramethylbenzidine (TMB) was purchased form Sigma-Aldrich (St Louis, USA) and dissolved in dimethyl sulfoxide (DMSO) to generate a freshly prepared stock solution (100 mM). 2,2'-azino-bis(3-ethylbenzothiazoline-6-sulfonic acid)diammonium salt (ABTS), dopamine hydrochloride, hydrogen peroxide (30 wt%) and all the acrylic monomers were also purchased from Sigma-Aldrich and dissolved freshly in water. Sodium chloride, sodium acetate, sodium dodecyl sulfate (SDS), acetic acid, and 4-(2-hydroxyethyl) piperazine-1-ethanesulfonate (HEPES) were from Mandel Scientific (Guelph, ON). Milli-Q water was used for all the experiments.

Preparation of Fe_3O_4 NPs and Other Nanozymes. Fe_3O_4 nanoparticles (NPs) were prepared following literature reported methods.[41] $FeCl_2$ (0.2 M, 1.0 mL) and $FeCl_3$ solutions (0.1 M, 4.0 mL) were mixed under nitrogen gas, to which aqueous ammonia (0.2 M, 15 mL) was added drop-wise under stirring. The mixture was heated at 80 °C for 1 h under nitrogen. After cooling to room temperature, the resulting Fe_3O_4 NPs were washed by Milli-Q water until the supernatant was clear (final yield: 70.3%). Gold nanoparticles (AuNPs, 13 nm) were synthesized using the citrate reduction procedures with a concentration of ~10 nM.[42] Nanoceria (CeO_2, size ~5 nm, 20 wt% dispersed in 2.5% acetic acid from Sigma-Aldrich, catalog number 289744) was diluted in buffer A (20 mM acetate, pH 4.0) for use.

Imprinting on nanozymes. All the imprinted nanogels were prepared using the aqueous precipitation polymerization method. In a typical reaction, Fe_3O_4 NPs (60 μg/mL) and a substrate to be imprinted (1 mM) were mixed in buffer B (20 mM HEPES, pH 7.6) for 30 min under N_2. Acrylamide (2.9 mg, 42 μmol), N-isopropylacrylamide (NIPAAm) (4.6 mg, 42 μmol), N,N'-methylenebisacrylamide (MBAAm as crosslinker) (2.4 mg, 16 μmol) and SDS (0.8 mg) were dissolved in 0.5 mL buffer B to prepare a monomer solution. For the charged gels, a function monomer, *N*-[3-(dimethylamino)propyl]methacrylamide (DMPA), or 2-

acrylamido-2-methyl-1-propanesulfonic acid (AMPS) (10 μmol) was also included in the monomer solution. The structures of the monomers are in Figure S1, Supporting Information. After purging the monomer solutions with N_2 for 1 h, polymerization was initiated by adding ammonium persulfate (0.2 mg) and tetramethyl-ethylenediamine (0.3 μL). The monomer and the Fe_3O_4-containing solutions were mixed after 20 min of initiation. The final reaction volume was standardized to 1 mL. The reaction was continued for 8 h at room temperature under nitrogen. The resulting imprinted gels were collected by centrifugation at 5,000 rpm for 10 min. Then 1 mM H_2O_2 was added to react with the imprinted substrates so they can be easily removed by subsequent washing using Milli-Q water. UV-vis spectroscopy was used to confirm fully washed nanogels. The imprinted gels were lyophilized for 24 h and weighed to determine the reaction yield. The nanogels were imprinted on AuNPs (10 nM) and nanoceria (100 μg/mL) using the same method. Non-imprinted nanogels (NIPs) were also prepared in the same way except that no substrate template was added. The incorporation efficiency of Fe_3O_4 NPs in nanogels were measured by comparing the UV-Vis peak at 400 nm (due to Fe_3O_4 NPs) of the supernatant after imprinting (indicative of non-incorporated NPs) and that of the free Fe_3O_4 NPs (60 μg/mL) before imprinting.

ICP-MS. To measure the Fe_3O_4 concentration in the nanogels, different nanogels (5 mg/mL) were dissolved in 5 % (w/v) nitric acid overnight. The dissolved solutions were then centrifuged at 15 000 rpm for 10 min and then filtered using 0.45 μm filters to remove the gel shells. Its iron concentration was measured by inductively-coupled plasma-mass spectrometry (ICP-MS, Thermo Fisher Xseries II).

TEM, SEM, EDX and DLS. The size and morphology of the nanogels were studied using transmission electron microscopy (TEM, Philips CM10). A gel dispersion (200 μg/mL) was drop-cast onto a copper grid and allowed to dry overnight at room temperature. For SEM, lyophilized samples were dropped on a conductive carbon tape for imaging using a LEO FESEM 1530 field-emission scanning electron microscope equipped with an EDAX Pegasus 1200 energy-dispersive X-ray analysis system (EDX). The size and ζ-potential of nanogels (50 μg/mL) were measured by dynamic light scattering (DLS) on a Zetasizer Nano ZS90 (Malvern) at 25 °C in buffer A.

ITC. ITC was performed using a VP-ITC microcalorimeter (MicroCal). Prior to measurement, each solution was degassed to remove air bubbles. The nanogels (5 mg/mL) dispersed in buffer A (containing 1 % v/v DMSO) was loaded in a 1.45 mL ITC cell at 25 °C. ABTS or TMB (280 μL, 2 mM) in the same buffer was titrated into the cell (20 μL each time, except for the first injection of 2 μL). The enthalpy (ΔH) and binding constant (K_a) were obtained through fitting the titration curves to a one-site binding model. The K_d values were calculated from $1/K_a$ and $\Delta G = -RT\ln(K_a)$, where R is the gas constant. ΔS was calculated from $\Delta G = \Delta H - T\Delta S$.

Activity assays. For a typical peroxidation reaction, a substrate (0.5 mM) was mixed with free Fe_3O_4 NPs (50 μg/mL) or imprinted nanogels (~5 mg/mL gel containing 50 μg/mL Fe_3O_4) in buffer A. The absorbance of the oxidization products (652 nm for TMB, 420 nm for ABTS, and 480 nm for dopamine) was followed after adding 10 mM H_2O_2 using an Agilent 8453A spectrometer at 25 °C. To measure the enzyme parameters, various concentrations of substrates (0.05, 0.1, 0.2, 0.3, 0.4, 0.5, 0.75, 1 mM) were used. The UV absorbance, A, was then converted to concentrations c, through Beer's law: $A = \varepsilon c l$ (ε = 39 000, 36 800, and 3058 M^{-1} cm^{-1} for the products of TMB, ABTS, and dopamine, respectively; l is the pathlength of 1 cm). The background oxidation was subtracted for all the kinetics. The oxidation rates (V) were obtained by fitting a straight line to the initial linear region of the kinetic curves. V_{max} and K_m were obtained by fitting the data with the Michaelis–Menten equation: $V = V_{max}[S]/(K_m + [S])$, and k_{cat} was calculated from $V_{max} = k_{cat}[E]$, where [S] and [E] are the concentrations of substrates and nanozyme respectively. With 50 μg/mL of Fe_3O_4 NPs, its molar concentration is 1.1 nM based on 30 nm diameter. The oxidation reactions by other nanozymes and their imprinted gels (nanoceria, 100 μg/mL; AuNPs, 10 nM) were tested in the same way.

Results and Discussion

Fe_3O_4 NPs as a peroxidase-mimicking nanozyme. Iron oxide NPs are among the first reported nanozymes with peroxidase-like activity.[1] We chose it because of its robust activity and excellent biocompatibility. We prepared Fe_3O_4 NPs using the hydrothermal method.[41] To confirm its peroxidase-like activity, we respectively mixed TMB and ABTS substrates with the Fe_3O_4 NPs and H_2O_2. A blue color was observed with TMB, and green color with ABTS, indicating both were oxidized (Figure 1A). Without the Fe_3O_4 NPs, no color change occurred for either compound, indicating the catalytic role of Fe_3O_4. If H_2O_2 was omitted, no color occurred with Fe_3O_4 NPs alone either, confirming Fe_3O_4 was a peroxidase-mimicking nanozyme.

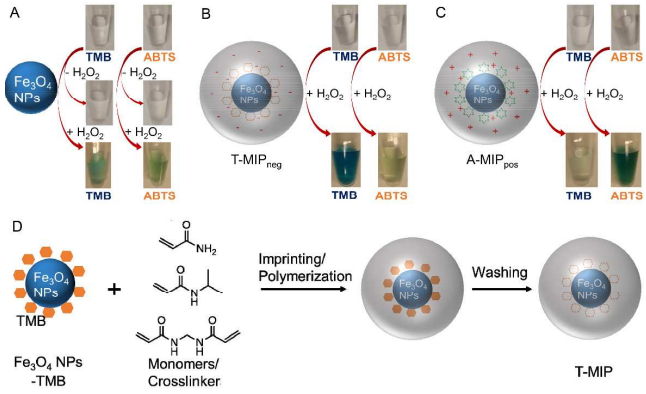

Figure 1. (A) Photographs showing the activity and specificity of (A) Fe_3O_4 NPs, (B) T-MIPneg and (C) A-MIPpos nanogels for oxidation of TMB and ABTS with or without H_2O_2. Fe_3O_4 NPs (50 μg/mL, free or in nanogels) were used in all experiments oxidizing 0.5 mM substrates with 10 mM H_2O_2 in buffer A (20 mM acetate, pH 4.0) for 30 min at room temperature. (D) A scheme of imprinting TMB on Fe_3O_4 NPs.

Imprinting on Fe_3O_4 NPs. Since Fe_3O_4 NPs can oxidize both TMB and ABTS in the presence of H_2O_2, it has poor substrate specificity. We hope to imprint substrate binding pockets on Fe_3O_4 NPs to selectively oxidize only one of them. To achieve this, we need to confirm that TMB and ABTS can be adsorbed on Fe_3O_4 NPs. We measured the ζ-potential of free Fe_3O_4 NPs to be -18.5 mV (Figure 2A). Adding positively charged TMB shifted the charge to -11.2 mV, suggesting TMB adsorption. The negatively charged ABTS further decreased the charge of Fe_3O_4, also suggesting adsorption. Therefore, at least a fraction of the added substrates were adsorbed by the Fe_3O_4 NPs to enable surface imprinting.

After confirming adsorption, we then added acrylamide and NIPAAm as monomers and MBAAm as a crosslinker to the Fe_3O_4 NPs and TMB (or ABTS) mixture. Note that H_2O_2 was

omitted to avoid oxidation. After adding initiators, this system underwent precipitation polymerization to yield nanogels.[12] The substrate template was then washed away to create binding pockets as shown in Figure 1D. A TEM micrograph of our Fe_3O_4 NPs is shown in Figure 2B. The average particle size is ~30 nm (Figure S2) and they appear aggregated. The catalytic activity of Fe_3O_4 relies on its native oxide surface and we avoided strong surface capping ligands during synthesis, which can explain the relatively large size distribution and tendency to aggregate (see Table S1 for more discussion on the synthesis).

After imprinting, the nanogel products appeared quite irregular under TEM likely due to drying in air (Figure 2C). The gel size distribution based on TEM was between 150-250 nm (Figure S3A). By zooming in on each particle, a darker feature in the middle indicative of a Fe_3O_4 NP core can be identified (inset of Figure 2C). From dynamic light scattering (DLS), these nanogels were well dispersed in water with an average hydrodynamic size of ~200 nm (Figure S4). This is consistent with our TEM data, suggesting drying on the TEM grid did not significantly shrinking the nanogels on the *x-y* plane likely due to its sticky gel nature. The polydispersity index (PDI) was ~0.3 for imprinted nanogels, which is significantly larger than that of the free nanogels without a Fe_3O_4 core (PDI ~0.1). Therefore, polymerization on the NPs has broadened the size distribution of the nanogels.

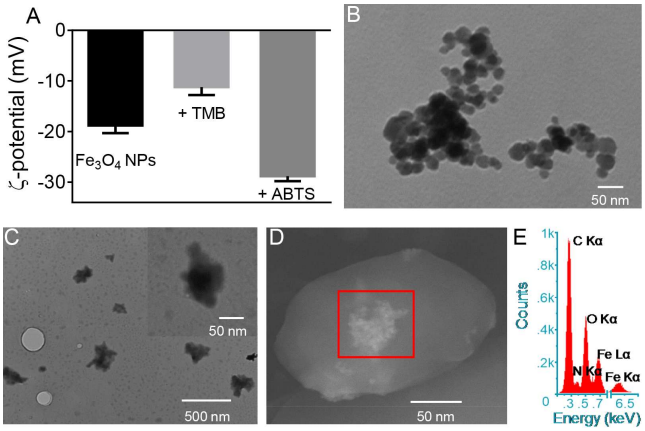

Figure 2. (A) ζ-potential of free Fe_3O_4 NPs in buffer B (20 mM HEPES buffer, pH 7.6) and after adding 1 mM TMB or ABTS. TEM micrographs of (B) free Fe_3O_4 NPs and (C) T-MIP nanogels. Inset of (C): a zoomed-in micrograph of a single nanogel showing the Fe_3O_4 NP core. (D) An SEM micrograph of a T-MIP nanogel and (E) its EDX elemental spectrum on the analyzed area defined by the red square. The gel was lyophilized to maintain its shape in (D), while the gel in (C) was dried on a TEM grid in air.

To further characterize the nanogels, SEM was measured on lyophilized samples (Figure 2D) showing the iron oxide core entrapped in the gel. The EDX spectrum indicates the presence of iron along with carbon, nitrogen and oxygen (Figure 2E). Our Fe_3O_4 NPs appeared brown with an absorption peak at 400 nm, which allowed us to measure its concentration (Figure S5). The iron incorporation efficiency in the nanogels was 83 ± 8 % by monitoring the 400 nm absorption peak. This is consistent with that determined by ICP-MS (81 ± 7 %) after dissolving the Fe_3O_4 NPs by nitric acid (Figure S6).

It is quite interesting that polymerization occurred around Fe_3O_4 NPs. This suggests that the monomers were also favorably adsorbed on the surface. The TMB and ABTS imprinted gels are named T-MIP and A-MIP, respectively. In addition, we also prepared the same nanogel but in the absence of TMB or ABTS. These negative control gels are named NIP for non-imprinted polymers (still containing the Fe_3O_4 core).

Imprinting enhances catalytic activity. After preparing these imprinted nanozymes, we next measured their activity. All the nanogels were standardized using UV-vis spectroscopy to contain the same concentration of Fe_3O_4 (50 μg/mL) regardless of free Fe_3O_4 NPs or nanogels. When TMB was catalyzed by free Fe_3O_4 NPs for 30 min, the absorption peak of the oxidation product at 652 nm reached 0.13 (Figure 3A, black trace). Next, the non-imprinted NIP sample was tested, and it has a similar activity (red trace). The gel layer might create a barrier for substrate accessibility, and one may expect decreased activity. Our results suggest that the gel was quite porous allowing efficient substrate diffusion to the surface. Therefore, the gel shell has no adverse influence on activity. Surface modification of nanozymes can sometimes even enhance activity. For example, Fan *et al* attached histidine to Fe_3O_4 NPs increasing its peroxidase-like activity by 20-fold.[43] We adsorbed fluoride on nanoceria increasing its oxidase-like turnover by nearly 100-fold.[11] Shen *et al* prepared MIP around TiO_2 photocatalyst also showing enhanced activity.[12]

After measuring these control samples, the TMB-imprinted nanogel (T-MIP) was then tested for TMB oxidation. It showed an increased absorbance reaching 0.23 (blue trace). Therefore, imprinted enhanced the activity by about one-fold. We next compared their reaction kinetics (Figure 3B), and a similar conclusion was obtained.

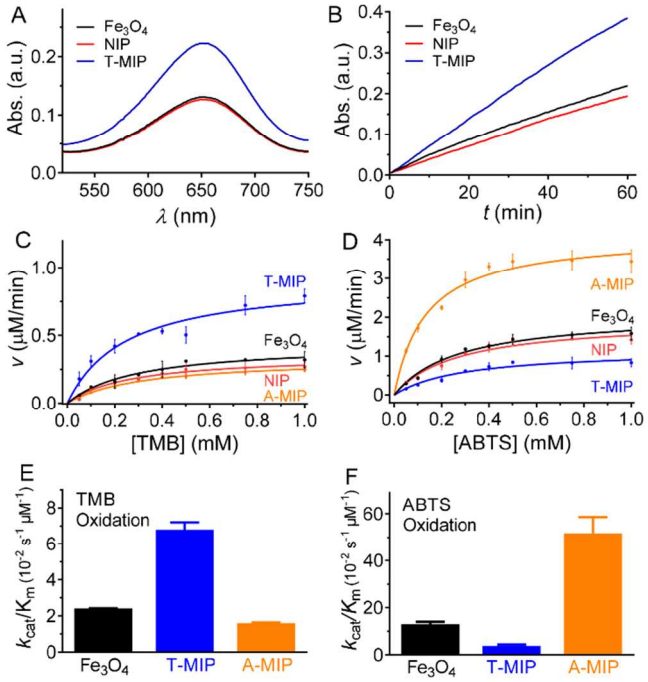

Figure 3. (A) UV-vis spectra after 30 min of TMB oxidation and (B) its kinetics monitored at 652 nm by free Fe_3O_4 NPs, NIP and T-MIP nanogels. Catalytic rates with various concentrations of (C) TMB and (D) ABTS by the free Fe_3O_4 NPs and different nanogels. The free Fe_3O_4 NPs and all the nanogels (~5 mg/mL) have the same concentration of Fe_3O_4 (50 μg/mL). All the reactions were with 10 mM H_2O_2 in buffer A at 25 °C. The catalytic efficiency (k_{cat}/K_m) of free Fe_3O_4 NPs and the

two imprinted gels (T-MIP and A-MIP) for oxidizing (E) TMB and (F) ABTS.

To test generality, we also imprinted with ABTS and the resulting nanogels are called A-MIP. Different from cationic TMB, ABTS is negatively charged. In this case, the A-MIP nanogel has an oxidation rate of 0.047 min^{-1}, 2.4-fold faster than that of the free Fe_3O_4 NPs (0.020 min^{-1}, Figure S7). Overall, the imprinted nanogels moderately enhanced the catalytic activity of Fe_3O_4 NPs for its imprinted target.

We next measured the rates of the nanozymes at various substrate concentrations to obtain enzyme parameters (Figure 3C, D). Based on the Michaelis-Menten model, their catalytic parameters are summarized in Table 1. The k_{cat} of T-MIP nanogel (15.0 s^{-1}) is more than twice that of free Fe_3O_4 NPs and A-MIP when oxidizing TMB. The T-MIP also has the highest affinity for TMB as indicated from its smallest K_m of 218 μM. For oxidizing ABTS, the A-MIP gel has the highest activity and affinity. Overall, the catalytic efficiency has enhanced towards their template targets by imprinting.

Table 1. Catalytic parameters of the free Fe_3O_4 NPs and the imprinted nanogels for oxidation of TMB and ABTS.[a]

Sub.	Enzyme	V_{max} (μM min^{-1})	k_{cat} (s^{-1})	K_m (μM)	k_{cat}/K_m (10^{-2} s^{-1} $μM^{-1}$)
TMB	Fe_3O_4	0.43 ± 0.04	7.1 ± 0.4	295 ± 30	2.4 ± 0.02
	NIP	0.36 ± 0.03	6.0 ± 0.3	266 ± 26	2.2 ± 0.05
	T-MIP	0.9 ± 0.04	15.0 ± 0.4	218 ± 24	6.8 ± 0.4
	T-MIPneg	3.4 ± 0.2	56.1 ± 1.7	150 ± 18	37.7 ±2.5
	A-MIP	0.3 ± 0.01	5.0 ± 0.08	316 ± 28	1.6 ± 0.1
	A-MIPpos	0.2 ± 0.04	3.3 ± 0.2	493 ± 26	0.7 ± 0.1
ABTS	Fe_3O_4	2.1 ± 0.1	35.0 ± 0.8	270 ± 34	12.9 ± 1.1
	NIP	1.9 ± 0.2	31.6 ± 1.8	267 ± 28	11.8 ± 0.03
	T-MIP	0.7 ± 0.05	11.6 ± 0.2	302 ± 26	3.8 ± 0.6
	T-MIPneg	0.4 ± 0.06	6.6 ± 0.2	360 ± 30	1.8 ± 0.02
	A-MIP	4.2 ± 0.2	70.1 ± 1.8	135 ± 22	51.8 ± 6.8
	A-MIPpos	6.5 ± 0.2	108.3 ± 1.7	93 ± 10	116.4 ± 9.5

[a] V_{max} is the maximal reaction velocity, k_{cat} is the catalytic constant, $k_{cat} = V_{max}/[E]$, the [E] is the molar concentration of Fe_3O_4 NPs (1.1 nM), and K_m is the Michaelis constant.

Imprinting enhances specificity. The enhance activity may lead to better specificity, which is the main goal of the current work. Next we measured specificity by also reacting the T-MIP gel with ABTS, and A-MIP with TMB. In general, the non-template substrate has lower activity than the template, (e.g. compare the orange and blue lines in Figure 3C, D). Therefore, with this simple imprinting process, substrate specificity was achieved.

To quantify specificity, we compared their catalytic efficiency k_{cat}/K_m.[44] T-MIP has 2.8-fold higher of k_{cat}/K_m (6.8×10^{-2} s^{-1} $μM^{-1}$) than that of bare Fe_3O_4 (2.4×10^{-2} s^{-1} $μM^{-1}$, Figure 3E). When oxidizing ABTS, the same gel showed ~3 times lower k_{cat}/K_m than bare Fe_3O_4 (Figure 3F). Similarly, the A-MIP has 4-fold higher specificity than bare Fe_3O_4 for oxidizing ABTS (Figure 3F), but 1.5-fold lower for oxidizing TMB (Figure 3E). Overall, imprinting using neutral acrylamide and NIPAAm as monomers achieved moderate selectivity.

Charged monomers drastically improve specificity and activity. Encouraged by the above results, we aimed to further improve imprinting by incorporating charged monomers, since TMB carries a positive charge and ABTS carries a negative charge. For this purpose, cationic DMPA or anionic AMPS was chosen as part of the monomer mixtures (Figure 4A). We then measured the zeta-potential of the resulting gels (Figure 4B). With more DMPA added, the gels became more positively charged, while AMPS has increased the negative charges, indicating that these monomers were successfully incorporated into the final nanogels. The charged nanogels were also larger (698 ± 21 nm), more than 3 times that of the non-charged ones (202 ± 19 nm, Figure S4). These charged gels swell more because of osmotic pressure and electrostatic repulsion related to the polyelectrolyte backbone.[45-47]

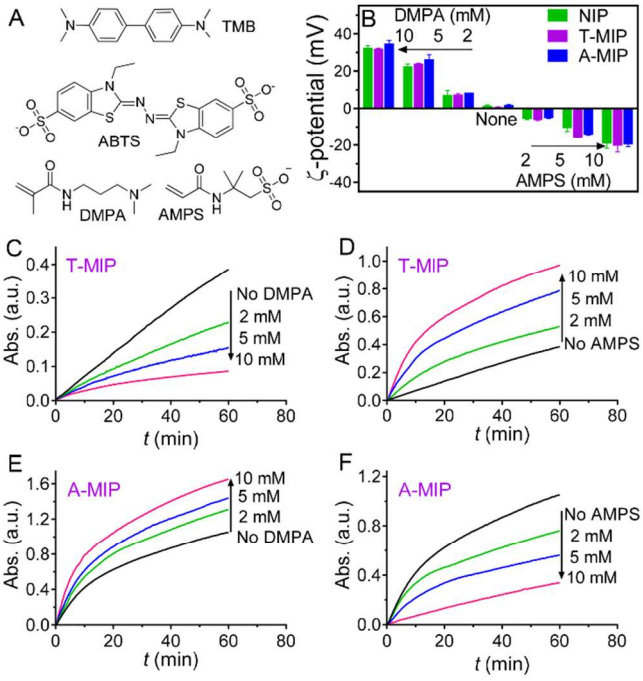

Figure 4. (A) The structure of the substrates and charged monomers. (B) The effect of charged monomers on the ζ-potential of the nanogels (50 μg/mL gels measured in buffer A at 25 °C). The kinetics of TMB (0.5 mM) oxidation monitored at 652 nm by the T-MIP nanogels containing 0-10 mM of (C) DMPA or (D) AMPS. (E, F) The kinetics of ABTS (0.5 mM) oxidation by the A-MIP nanogels containing charged monomers measured at 420 mm. All the nanogels in the activity tests were ~5 mg/mL containing same concentration of Fe_3O_4 (50 μg/mL) with 10 mM H_2O_2 in buffer A at 25 °C.

We next measured the activity of these charged nanogels. The activity of TMB imprinted nanogels for TMB oxidation dropped with more cationic DMPA added, since imprinting cationic TMB was disfavored by the cationic monomer (Figure 4C). On the other hand, its rate of TMB oxidation enhanced with more anionic AMPS incorporated (Figure 4D). Similarly, when ABTS was used for imprinting, cationic DMPA increased its oxidation rate (Figure 4E), while AMPS decreased it (Figure 4F). Therefore, charged monomers can further modulate the activity and thus specificity.

For the samples we tested so far, those with 10 mM charged monomers had the best activity for the oppositely charged template. Therefore, we used them for further studies. The TMB imprinted nanogels are named T-MIPneg if containing anionic AMPS, and named T-MIPpos if containing cationic DMPA. Those imprinted gels with ABTS are named in a similar way but starting with 'A-'. Next, we quantitatively measured their kinetic parameters (Figure 5A, B), and the k_{cat} and K_m values are presented in Table 1.

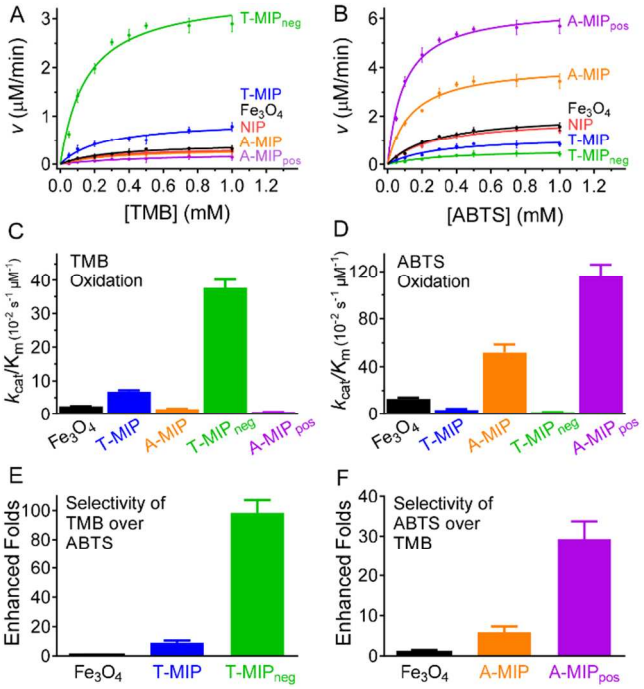

Figure 5. Catalytic rates in the presence of various concentrations of (A) TMB and (B) ABTS substrates by the free Fe_3O_4 NPs and different nanogels. The catalytic specificity (k_{cat}/K_m) of free Fe_3O_4 NPs and the four imprinted nanogels for oxidizing (C) TMB and (D) ABTS. The fold of specificity enhancement of (E) bare Fe_3O_4 NPs, T-MIP, T-MIPneg oxidizing TMB over ABTS and (F) bare Fe_3O_4 NPs, A-MIP, A-MIPpos oxidizing ABTS over TMB. The enhancement was calculated using normalized k_{cat}/K_m of oxidizing TMB divided that oxidizing ABTS.

Using TMB oxidation as an example, the k_{cat} value increased by 7.9-fold with the T-MIPneg gel compared to that with free Fe_3O_4, while the A-MIPpos gel even suppressed the activity by ~50%. At the same time, the K_m dropped by 50% for the T-MIPneg, suggesting even tighter substrate binding. We plotted k_{cat}/K_m of these imprinted nanozymes to compare enzyme specificity (Figure 5C and 5D). The T-MIPneg has the best catalytic efficiency, 15-fold higher than that of the bare Fe_3O_4 NPs, much better than the 3-fold improvement for the T-MIP gel without the negative AMPS monomer (Figure 5C). At the same time, the T-MIPneg has the least efficiency for ABTS oxidation (Figure 5D). The same trend was also observed for the A-MIPpos gel. In the best case, the selectivity for TMB over ABTS using the T-MIPneg nanogel is 98-fold (Figure 5E), while the selectivity for ABTS over TMB using the A-MIPpos is 33-fold (Figure 5F). These results are reflected from visual colorimetric tests showing we can now selectively oxidize either substrate by tuning monomer composition and imprinting (Figure 1B and C).

Binding thermodynamics. The above measurements were performed only using activity assays. The significantly enhanced specificity suggests successfully engineered substrate binding pockets. To further confirm this, and to understand the thermodynamics of binding, isothermal titration calorimetry (ITC) was employed. In this experiment, TMB or ABTS was gradually titrated into the imprinted or non-imprinted nanogels, and the amount of heat released was recorded as a function of time (Figure 6, top panels). Most reactions released heat, which was favorable for binding. The binding site of the nanogels is ~0.4 mM as determined by UV spectroscopy after imprinting. By integrating the heat (the lower panels), we directly calculated the enthalpy and dissociation constant, K_d, of the reaction. Then the ΔG and ΔS were calculated. These thermodynamic values are listed in Table 2.

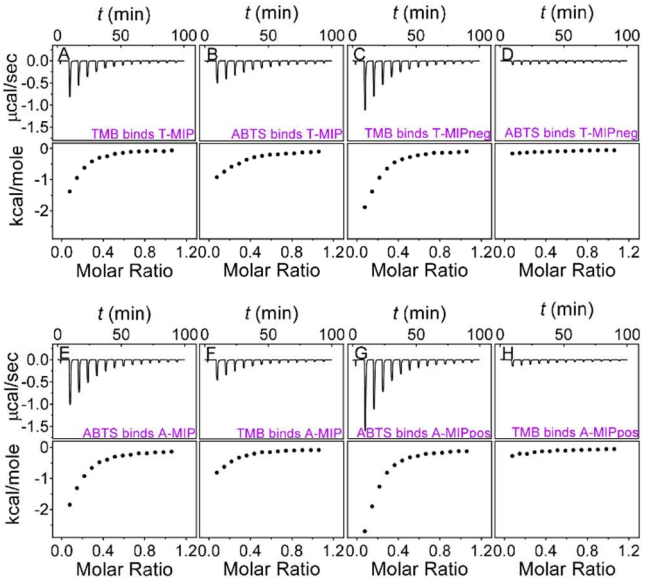

Figure 6. ITC traces at 298 K for binding TMB or ABTS by (A, B) T-MIP, (C, D) T-MIPneg, (E, F) A-MIP and (G, H) A-MIPpos nanogels. TMB and ABTS (2 mM) and the nanogels (5.0 mg/mL) were dispersed in buffer A with 1% v/v DMSO. The original titration traces (top) and the integrated heat (below) of each reaction are shown.

The T-MIP nanogels released more heat with a stronger affinity for binding TMB (Figure 6A, K_d = 27 μM) than binding ABTS (Figure 6B, K_d = 142 μM) indicating enhanced bind specificity through imprinting. After incorporating charged monomers (T-MIPneg, Figure 6C and D), the binding specificity was significantly enhanced with the highest heat released and strongest affinity for TMB (Figure 6C, K_d = 20 μM) over ABTS (Figure 6D, no measurable binding). For ABTS imprinted gels (A-MIP and A-MIPpos), more favorable binding to

ABTS was also observed (Figure 6E-H, Table 2). In general, charged monomers led to more heat release (e.g. enthalpy change). Imprinting can enhance binding affinity and selectivity to the imprinted substrates, and charged monomers further improve specificity, which explains the enhanced nanozyme specificity after imprinting.

Table 2. The thermodynamic parameters of the imprinted gels calculated from ITC.

Subs.	Gel samples	K_a ($\times 10^4$ M^{-1})	K_d (μM)	ΔG (kcal mol^{-1})	ΔH (kcal mol^{-1})	ΔS (cal $K^{-1}mol^{-1}$)
TMB	T-MIP	3.6 ±0.2	27.8 ±1.5	-6.1	-1.8 ±0.1	14.8
	T-MIPneg	4.8 ±0.2	20.8 ±0.8	-6.3	-2.7 ±0.2	12.4
	A-MIP	0.8 ±0.1	125.0 ±15.9	-5.3	-1.2 ±0.1	13.8
	A-MIPpos	-[b]	-	-	-0.3 ±0.02	-
ABTS	T-MIP	0.7 ±0.06	142.8 ±12.4	-5.2	-1.3 ±0.05	13.2
	T-MIPneg	-	-	-	-0.2 ±0.01	-
	A-MIP	3.9 ±0.2	25.6 ±1.3	-6.2	-2.6 ±0.1	12.2
	A-MIPpos	5.7 ±0.5	17.5 ±1.6	-6.4	-3.2 ±0.3	11.0

Notes: [a] The binding data were obtained using a one-site binding model. [b] Binding (K_a < 1000 M^{-1}) was not detectable by ITC.

Imprinting on other nanozymes. So far, all our work was focused on Fe_3O_4 NPs. To test the generality of this approach, we next tried two more nanozymes: nanoceria (CeO_2) mimicking oxidase activity,[20,48,49] and AuNPs mimicking peroxidase.[50,51] Different from Fe_3O_4 NPs, nanoceria can oxidize TMB and ABTS in the absence of H_2O_2 (e.g. oxidase). Therefore, these substrates are oxidized upon mixing with nanoceria, making it difficult for imprinting. Fortunately, the optimal pH for nanoceria is at pH 4.[20] Indeed, we confirmed that nanoceria is essentially non-active at pH 7.6 (20 mM HEPES, nitrogen atmosphere) (Figure S8), allowing imprint on nanoceria at pH 7.6.

These imprinted nanoceria containing gels also have a size of ~210 nm similar to that of Fe_3O_4 containing nanogels (Figure S9), indicating that the growth of the gel is quite independent of the core composition. The morphology of the nanoceria imprinted gels were characterized by TEM (Figure 7A), confirming the presence of the nanozyme core. Then we measured the activity of oxidizing TMB by free nanoceria and by different nanogels (Figure 7C). After imprinting, the activity of nanoceria increased by ~1.7-fold with T-MIP and more than 3-fold with T-MIPneg containing AMPS (Figure 7C). At the same time, these gels suppressed the for ABTS oxidation (Figure S10A) indicating the substrate selectivity was also achieved for nanoceria after imprinting.

Fe_3O_4 and nanoceria are both metal oxides, and we next tested a different type of material, AuNPs, which are also peroxidase mimics requiring H_2O_2.[50,51] We respectively imprinted 13 nm AuNPs with two substrates: TMB and dopamine. ABTS was not used since AuNPs cannot oxidize ABTS in the presence of H_2O_2. The dopamine imprinted nanogels were named using the same method starting with 'D-'. The gels were also characterized by TEM confirming incorporation of AuNPs (Figure 7B). The enhanced activity and specificity was also observed (Figure 7D and Figure S10B). For example, the T-MIPneg showed the highest enhancement of 2.9-fold compared to free AuNPs. Since dopamine has a positive charge in the test condition (pH 4.0), its best activity was observed with the D-MIPneg (Figure S10B).

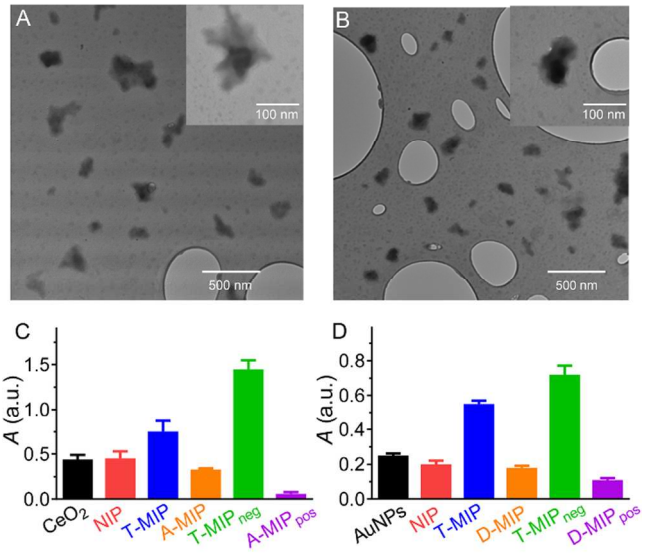

Figure 7. TEM micrographs of (A) nanoceria and (B) AuNPs imprinted T-MIP nanogels. The inserts are zoomed in pictures of single nanogels. Oxidation of TMB by (C) free nanoceria (100 μg/mL), (B) AuNPs (10 nM) and different gels measured at 652 nm. All the gels (~5 mg/mL) have same concentration of CeO_2 or the AuNPs. All the measurements were in buffer A at 25 °C.

We have so far tested three nanozymes covering two types of materials (metal and metal oxide), two types of activities (oxidase and peroxidase), and three types of substrates (TMB, ABTS and dopamine), all showing a consistent effect of molecular imprinting. These results indicate that molecular imprinting is a general method for enhancing activity and specificity. Molecular imprinting was previously performed on TiO_2 to remove toxic pollutants, but specificity was not tested.[12,35-38] Some protein enzymes such as the horseradish peroxidase (HRP) are quite non-specific and it accepts a broad range of substrates.[52] For example, HRP has a K_m of 434 μM for TMB,[1,53] and 138 μM for ABTS, and the catalytic efficiencies for these two substrates are similar.[54] Using a similarly non-specific peroxidase mimicking Fe_3O_4, we demonstrated excellent specificity even better than some natural enzymes. For example, the K_m of T-MIPneg for TMB is 2.9-fold lower than that of HRP, and the K_m of A-MIPpos for ABTS is also 1.5-fold lower (Table 1). The improvement in specificity (defined by k_{cat}/K_m) is even more significant.

In other cases, however, our ~100-fold selectivity still falls behind natural enzymes. Enzymes use a suite of mechanisms to achieve exquisite specificity, such as uniform and well-defined substrate binding pockets, proofreading, and dynamic conformational changes. As the first step here, we only imprinted the substrate shape with simple electrostatic modulation in this case. There is a lot more to learn from nature in

future work by also incorporating other molecular recognition mechanisms.

Conclusions.

Nanozymes promise to provide functional mimics of enzymes using cost-effective and robust inorganic materials. By using similarly cost-effective and robust MIPs, we solved an intrinsic problem of the nanozyme: lack of specificity. With molecular imprinting, we successfully engineered substrate binding pockets on three different nanozymes. By incorporating functional monomers with charges, the activity and specificity were further improved. Under optimal conditions, specificity can reach ~100 fold. Selective substrate binding was confirmed by ITC and its thermodynamic parameters were obtained for fundamental insights. With good enzyme specificity, more advanced applications of nanozymes can be realized, including biosensors with the MIP layer as receptors, selective destruction of disease causing molecules and environmental contaminants, and delivery of therapeutic agents.

ASSOCIATED CONTENT

Supporting Information

Materials and methods, controls, DLS, UV-vis, ICP-MS data and biochemical assays. This material is available free of charge via the Internet at http://pubs.acs.org.
(PDF)

AUTHOR INFORMATION

Corresponding Author

Email: liujw@uwaterloo.ca

Notes

The authors declare no competing financial interests.

ACKNOWLEDGMENT

This work is supported by the Natural Sciences and Engineering Research Council of Canada (NSERC), Strategic Project Grant (STPGP 447472-13).

REFERENCES

(1) Gao, L.; Zhuang, J.; Nie, L.; Zhang, J.; Zhang, Y.; Gu, N.; Wang, T.; Feng, J.; Yang, D.; Perrett, S.; Yan, X. *Nat. Nanotechnol.* **2007**, *2*, 577.
(2) Wei, H.; Wang, E. *Chem. Soc. Rev.* **2013**, *42*, 6060.
(3) Lin, Y. H.; Ren, J. S.; Qu, X. G. *Acc. Chem. Res.* **2014**, *47*, 1097.
(4) Wang, X.; Hu, Y.; Wei, H. *Inorg. Chem. Front.* **2016**, *3*, 41.
(5) Lin, Y. H.; Ren, J. S.; Qu, X. G. *Adv. Mater.* **2014**, *26*, 4200.
(6) Gao, L. Z.; Yan, X. Y. *Sci. China Life Sci.* **2016**, *59*, 400.
(7) Liu, B.; Liu, J. *Nano Res.* **2017**, 1.
(8) Zheng, X.; Liu, Q.; Jing, C.; Li, Y.; Li, D.; Luo, W.; Wen, Y.; He, Y.; Huang, Q.; Long, Y.-T.; Fan, C. *Angew. Chem., Int. Ed.* **2011**, *50*, 11994.
(9) Luo, W.; Zhu, C.; Su, S.; Li, D.; He, Y.; Huang, Q.; Fan, C. *ACS Nano* **2010**, *4*, 7451.
(10) Liang, M. M.; Fan, K. L.; Pan, Y.; Jiang, H.; Wang, F.; Yang, D. L.; Lu, D.; Feng, J.; Zhao, J. J.; Yang, L.; Yan, X. Y. *Anal. Chem.* **2013**, *85*, 308.
(11) Liu, B.; Huang, Z.; Liu, J. *Nanoscale* **2016**, *8*, 13562.
(12) Shen, X.; Zhu, L.; Liu, G.; Tang, H.; Liu, S.; Li, W. *New J. Chem.* **2009**, *33*, 2278.
(13) Wang, N.; Zhu, L. H.; Wang, D. L.; Wang, M. Q.; Lin, Z. F.; Tang, H. Q. *Ultrasonics Sonochem.* **2010**, *17*, 526.
(14) Huang, Y. Y.; Liu, Z.; Liu, C. Q.; Ju, E. G.; Zhang, Y.; Ren, J. S.; Qu, X. G. *Angew. Chem. Int. Ed.* **2016**, *55*, 6645.
(15) Gao, N.; Dong, K.; Zhao, A. D.; Sun, H. J.; Wang, Y.; Ren, J. S.; Qu, X. G. *Nano Res.* **2016**, *9*, 1079.
(16) Chen, Z.; Yin, J.-J.; Zhou, Y.-T.; Zhang, Y.; Song, L.; Song, M.; Hu, S.; Gu, N. *ACS Nano* **2012**, *6*, 4001.
(17) Cheng, H.; Zhang, L.; He, J.; Guo, W.; Zhou, Z.; Zhang, X.; Nie, S.; Wei, H. *Anal. Chem.* **2016**, *88*, 5489.
(18) Celardo, I.; Pedersen, J. Z.; Traversa, E.; Ghibelli, L. *Nanoscale* **2011**, *3*, 1411.
(19) Fan, K. L.; Cao, C. Q.; Pan, Y. X.; Lu, D.; Yang, D. L.; Feng, J.; Song, L. N.; Liang, M. M.; Yan, X. Y. *Nat. Nanotechnol.* **2012**, *7*, 459.
(20) Asati, A.; Santra, S.; Kaittanis, C.; Nath, S.; Perez, J. M. *Angew. Chem., Int. Ed.* **2009**, *48*, 2308.
(21) Comotti, M.; Della Pina, C.; Matarrese, R.; Rossi, M. *Angew. Chem., Int. Ed.* **2004**, *43*, 5812.
(22) Liu, Y.; Purich, D. L.; Wu, C. C.; Wu, Y.; Chen, T.; Cui, C.; Zhang, L. Q.; Cansiz, S.; Hou, W. J.; Wang, Y. Y.; Yang, S. Y.; Tan, W. H. *J. Am. Chem. Soc.* **2015**, *137*, 14952.
(23) Cai, R.; Yang, D.; Peng, S. J.; Chen, X. G.; Huang, Y.; Liu, Y.; Hou, W. J.; Yang, S. Y.; Liu, Z. B.; Tan, W. H. *J. Am. Chem. Soc.* **2015**, *137*, 13957.
(24) Zhang, L.; Han, L.; Hu, P.; Wang, L.; Dong, S. *Chem. Commun.* **2013**, *49*, 10480.
(25) Pirmohamed, T.; Dowding, J. M.; Singh, S.; Wasserman, B.; Heckert, E.; Karakoti, A. S.; King, J. E. S.; Seal, S.; Self, W. T. *Chem. Commun.* **2010**, *46*, 2736.
(26) Korsvik, C.; Patil, S.; Seal, S.; Self, W. T. *Chem. Commun.* **2007**, 1056.
(27) Liang, H.; Lin, F.; Zhang, Z.; Liu, B.; Jiang, S.; Yuan, Q.; Liu, J. *ACS Appl. Mater. Inter.* **2017**, *9*, 1352.
(28) Golub, E.; Albada, H. B.; Liao, W.-C.; Biniuri, Y.; Willner, I. *J. Am. Chem. Soc.* **2016**, *138*, 164.
(29) Schirhagl, R. *Anal. Chem.* **2014**, *86*, 250.
(30) Wulff, G. *Angew. Chem., Int. Ed.* **1995**, *34*, 1812.
(31) Haupt, K.; Mosbach, K. *Chem. Rev.* **2000**, *100*, 2495.
(32) Chen, L.; Xu, S.; Li, J. *Chem. Soc. Rev.* **2011**, *40*, 2922.
(33) Cheong, W. J.; Yang, S. H.; Ali, F. *J. Sep. Sci.* **2013**, *36*, 609.
(34) Volkert, A. A.; Haes, A. J. *Analyst* **2014**, *139*, 21.
(35) Shen, X. T.; Zhu, L. H.; Wang, N.; Zhang, T.; Tang, H. Q. *Catalysis Today* **2014**, *225*, 164.
(36) Li, Y. X.; Li, Y. J.; Huang, L. H.; Bin, Q.; Lin, Z. Y.; Yang, H. H.; Cai, Z. W.; Chen, G. N. *J. Mater. Chem. B* **2013**, *1*, 1256.
(37) Wulff, G.; Liu, J. Q. *Acc. Chem. Res.* **2012**, *45*, 239.
(38) Shen, X. T.; Zhu, L. H.; Huang, C. X.; Tang, H. Q.; Yu, Z. W.; Deng, F. *J. Mater. Chem.* **2009**, *19*, 4843.
(39) Liu, J.-q.; Wulff, G. *Angew. Chem., Int. Ed.* **2004**, *43*, 1287.
(40) Zhang, Z.; Liu, B.; Liu, J. *Small* **2016**, 1602730.
(41) Philipse, A. P.; van Bruggen, M. P. B.; Pathmamanoharan, C. *Langmuir* **1994**, *10*, 92.
(42) Liu, J.; Lu, Y. *Nat. Protoc.* **2006**, *1*, 246.
(43) Fan, K.; Wang, H.; Xi, J.; Liu, Q.; Meng, X.; Duan, D.; Gao, L.; Yan, X. *Chem. Commun.* **2017**, *53*, 424.
(44) Hedstrom, L. In *eLS*; John Wiley & Sons, Ltd: 2001.
(45) De, S. K.; Aluru, N. R.; Johnson, B.; Crone, W. C.; Beebe, D. J.; Moore, J. *J. Microelectromech. Sys.* **2002**, *11*, 544.
(46) Rubinstein, M.; Colby, R. H.; Dobrynin, A. V.; Joanny, J. F. *Macromolecules* **1996**, *29*, 398.
(47) Joseph, K. A.; Dave, N.; Liu, J. *ACS Appl. Mater. Inter.* **2011**, *3*, 733.
(48) Peng, Y.; Chen, X.; Yi, G.; Gao, Z. *Chem. Commun.* **2011**, *47*, 2916.
(49) Xu, C.; Qu, X. *NPG Asia Mater* **2014**, *6*, e90.
(50) Jv, Y.; Li, B. X.; Cao, R. *Chem. Commun.* **2010**, *46*, 8017.
(51) Wang, S.; Chen, W.; Liu, A.-L.; Hong, L.; Deng, H.-H.; Lin, X.-H. *ChemPhysChem* **2012**, *13*, 1199.
(52) Morawski, B.; Quan, S.; Arnold, F. H. *Biotechnol.Bioeng.* **2001**, *76*, 99.
(53) Guo, Y.; Deng, L.; Li, J.; Guo, S.; Wang, E.; Dong, S. *ACS Nano* **2011**, *5*, 1282.
(54) O'Brien, A. M.; Smith, A. T.; Ó'Fágáin, C. *Biotechnol. Bioeng.* **2003**, *81*, 233.

For Table of Content Graphics Only